Transient Analysis of the Buoyancy Driven Flow in a Passive Solar System for Indoor Heating

Cammarata G., Petrone G.*, Cammarata L.
Department of Industrial and Mechanical Engineering - University of Catania
*Corresponding author: Viale A. Doria, 6 – 95125 Catania, gpetrone@diim.unict.it

Abstract: This study aims to numerically investigate on a passive solar system for indoor heating called as "Trombe wall". The transient buoyancy driven flow characterizing that system and the thermal distribution are solved by numerically integrating the governing equations in COMSOL Multiphysics environment. Simulations are carried-out for a time range corresponding to 12 days. The results are summarized in motion fields and thermal maps, that are critically discussed together with phenomenological aspects concerning thermal efficiency of the storage system and comfort conditions inside the considered indoor environment.

Keywords: Natural convection, HVAC systems, solar energy, "Trombe wall".

1. Introduction

In the framework of renewable energy for application in HVAC systems (Heating, Ventilation and Air Conditioning), a growing interest is more and more dedicated to the passive solar systems [1-6]. Those systems are so called because any mechanical devises is involved in their functioning, neither for solar energy pick up nor for indoor air ventilation. Among the passive solar systems, one of the most known is the "Trombe wall". In a "Trombe wall" a glazing is installed at a small distance from a massive wall. The wall absorbs solar radiation and transmits a part of it into the interior of the building by natural convection through a solar chimney formed by the glazing on one side and the wall on the other side. The functional principle is based on a thermo-circulation phenomenon: the massive wall absorbs the solar flux through the glazing. The wall transfers a part of the flux inside the building by conduction. The heating of the air in contact with this wall induces a natural circulation: the air is admitted by the lower vent of the wall and comes back to the room by the upper vent. The air circulating, transfers part of the solar heat flux. In this paper a numerical study aimed to investigate on thermal and fluid-dynamical behavior of a "Trombe wall" system is proposed.

2. Numerical model

The geometry of the numerical model is represented in Figure 1. The structural elements of the system are filled with different colors: red for brick, blue for glazing, gray for concrete and yellow for insulating material. The cyan filled geometry is representative of the air contained inside the room and circulating into the horizontal and inclined channels of the "Trombe wall" system.

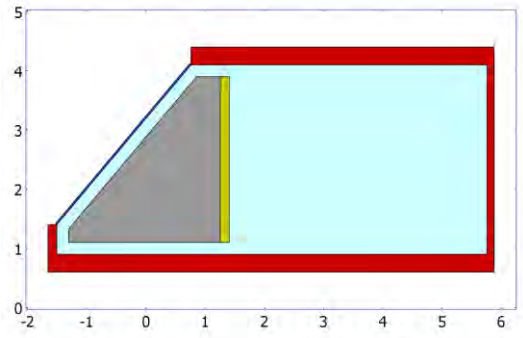

Figure 1. Geometry of the numerical model.

The governing equations for the physical system are momentum, mass and energy conservation equations. Under assumption of uncompressible fluid and laminar flow, they read as in following:

$$\rho\frac{\partial \mathbf{u}}{\partial t}+\rho(\mathbf{u}\cdot\nabla)\mathbf{u}=\nabla\cdot\left[-p\mathbf{I}+\eta(\nabla\mathbf{u})\right]+\mathbf{F}_g$$

$$\nabla\cdot(\rho\mathbf{u})=0$$

$$\rho C_P\frac{\partial T}{\partial t}+\nabla\cdot(-k\nabla T)+\rho C_p\mathbf{u}\cdot\nabla T=0$$

The source term in the momentum equation is the buoyancy force. By applying the ideal gas law, density of air is considered as a linear function of the temperature. Thermo-physical properties of materials used in computations are reported in Table 1.

	k	ρ	Cp
	[W(/m*K)]	[kg/m^3]	[J/(kg*K)]
Concrete	1,8	2400	1000
Brick	0,8	2685	790
Glazing	1,38	3150	795
Insulation	0,028	35	1400

	k	ρ	Cp	η
	[W/(m*K)]	[kg/m^3]	[J/(kg*K)]	[Pa*s]
Air	0,026	p_0/(R*T)	1010	1E-5

Table 1: Thermo-physical properties of structural materials and air.

The adherence condition at solid walls (blue in Figure 3) is adopted as boundary conditions in fluid-dynamical equations.

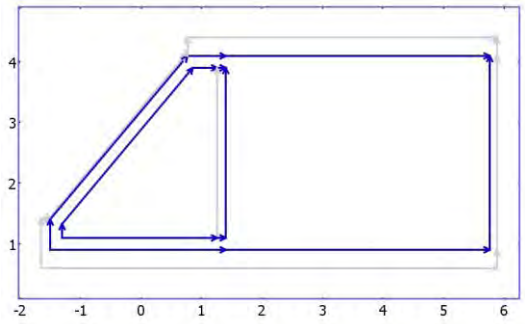

Figure 2. Boundary condition for fluid-dynamics.

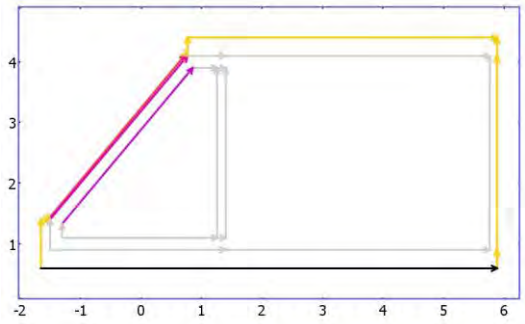

Figure 3. Boundary condition for thermal analysis.

Concerning energy equations, the applied boundary conditions (see Figure 3) can be listed as in following: insulation (black), continuity (grey), convective heat flux (yellow), imposed heat flux (pink). On the internal boundary represented in magenta "surface-to-surface" radiating condition is applied. Figure 4 reports, by the red-line, the 24-hours evolution of the imposed heat flux on the external surface of the glazing. In the same figure, by the black-line, it is indicated the 24-hours evolution of the external temperature adopted in the convective heat flux boundary condition. In that expression, the convective coefficient value is 22 [Wm^{-2}K^{-1}]. External temperature and solar flux are referred to the locality of Catania (south of Italy), latitude 37°30', during a winter day (extrapolated by the Whillier-Bliss method from data referring to the 1st December 2009).

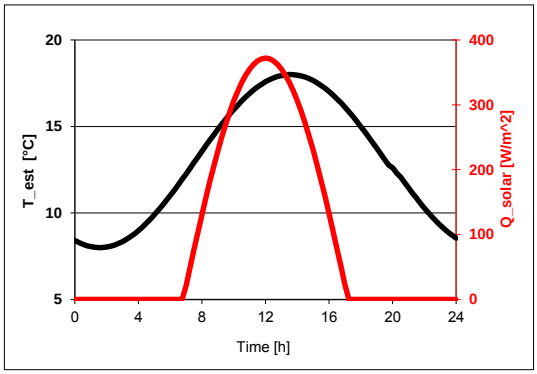

Figure 4. External temperature (black) and solar flux (red) time evolutions in 24 hours.

Continuous equations are discretized on a no-structured computational mesh made by triangular elements and using 2nd order shape functions. Time integration of discrete equations lies on a fractioned time step Backward Differentiation Formula scheme, where a modified Newton-Raphson method, at each time step, determinates a system of algebraic equations solved by the Unsymmetrical Multi-Frontal Package. Validation of the numerical tool in solving the system of interest is performed by comparing a preliminary test-case, built-up in COMSOL Multiphysics environment, in accordance with a "Trombe wall" system studied by another author [5] using the code TRNSYS.

An extract of the comparison is presented in Figure 5, where the time evolutions of external temperature (red line), reference internal temperature (green line) and computed average indoor temperature (blue line) are reported. The maximum relative difference is 8%. It is to notice that the reference data come from a numerical analysis made by a concentrated parameter code (one vale, at each time step, for the indoor temperature), while the compared data is computed, by a surface integration, as average value (at each time step) of the two-dimensional distribution of indoor air temperature.

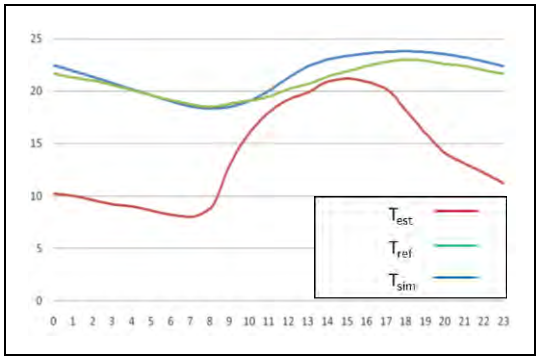

Figure 5. Extract of comparison between the present study and literature results [5].

3. Results

Simulations are done during 12 days and solutions are stored each 300 seconds. External thermal loads (solar flux and external temperature) are periodically applied for 24-hours periods. Computations are initialized by considering stagnant conditions for fluid and chosen temperature (8.54 °C) in all domains. Figure 6 show time evolutions of temperature, computed in a central point of the room (x=3.5; y=2.5), for each one of the 12 days simulated. In the same diagram, the external temperature 24-hours evolution is plotted also. It appears as, after 10 days elapsed, time evolution of temperature does not vary significantly from a day to another one. At the 12^{th} day the system assumes a not variant 24-hours evolution from a day to the day after. The system achieves a "stabilized" 24-hours evolution. This assumption is supported by the diagram reported in Figure 7, where the relative difference between a day to the previous one of temperature value (computed in x=3.5; y=2.5 at 00:00) is reported. From Figure 7 the saturation of the diagrammed parameter with increasing in time of simulation appears clearly.

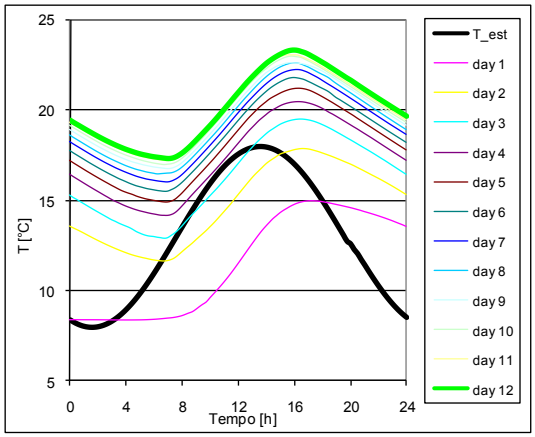

Figure 6. Time evolutions of the indoor temperature (x=3.5; y=2.5) during the 12 days of simulation. External temperature is also reported.

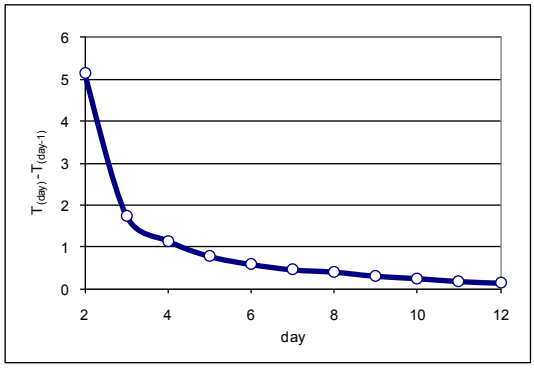

Figure 7. Relative difference of temperature value computed in x=3.5; y=2.5 at 00:00 between a day and the previous one.

From Figure 6 analysis, at the 12^{th} day a peak-to-peak displacement of the reported temperature evolution with respect to the external one can be observed. The time delay amounts to 5.5 hours about for the minimum and to 2.5 hours about for the maximum. In addition, indoor temperature level is increased with respect to external condition, varying in the range 17-23 °C. It appears as the minimum value of indoor temperature during the 24-hours is close by the maximum value of the external one. Let now

spend attention on the fluid-dynamical behavior of the system. At initial condition, fluid is stagnant. When heated, driven by the buoyancy effect, fluid starts to flow through the inclined and horizontal upper portion of the channel joining the room volume. A macroscopic clockwise circulation of air is detected inside the room. The fluid is then blown to the bottom horizontal channel, when it is heated again. Variation of thermal flux during the day is traduced in pulsating thermo-syphon circulation. Figures 8 and 9 report, in a color scale, the 12th day magnitude of velocity computed at time 00:00 and 12:00. The maximum value of the magnitude of air velocity (about 0.15 m/s) is detected inside the inclined channel. In room volume, magnitude of velocity is globally very low (less than 0.05 m/s), avoiding potential risk of discomforting draft effect for occupants.

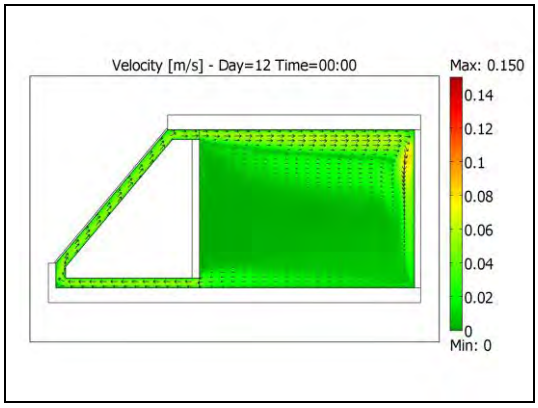

Figure 8. Magnitude of velocity (day 12 – time 00:00).

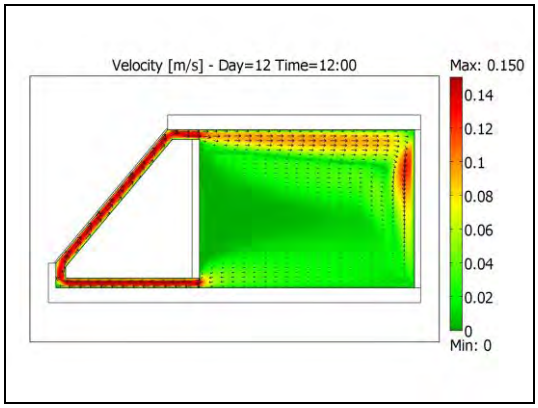

Figure 9. Magnitude of velocity (day 12 – time 12:00).

Peaks of velocity inside the room (0.1-0.12 m/s) occurs in fact close to the roof and to the right wall only. Referring to the channel width (0.2 m) the maximum Reynolds number evaluated is about 3000, that confirms the adopted hypothesis of laminar flow. Thermal maps, computed during the 12th day, are reported in Figures 10-13 at different hours. Thermal storage in the concrete mass is clearly observable, as well as thermal transport assured by the fluid motion in the upper portion of the air volume. As all thermal system whose functional principle is based on natural convection, thermal stratification of air with respect to the height happens. Referring to thermal comfort of occupants, this is a damaging occurrence. In order to better underline this aspect, indoor air temperature map is plotted when distribution of thermal levels reaches its maximum heterogeneity (time 16:00, Figure 14).

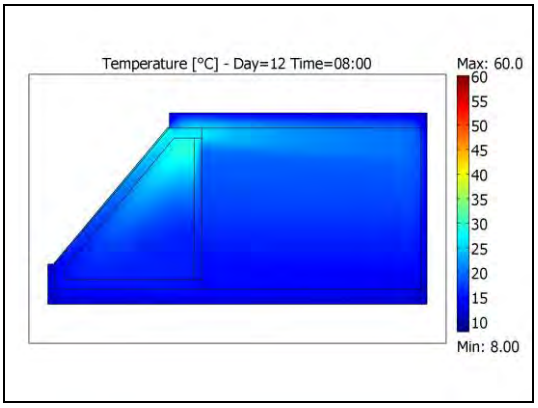

Figure 10. Thermal map (day 12 – time 08:00).

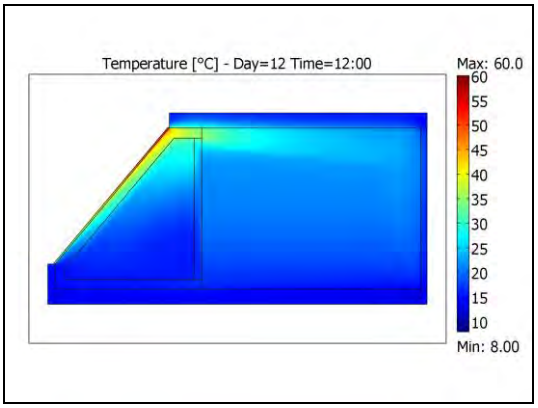

Figure 11. Thermal map (day 12 – time 12:00).

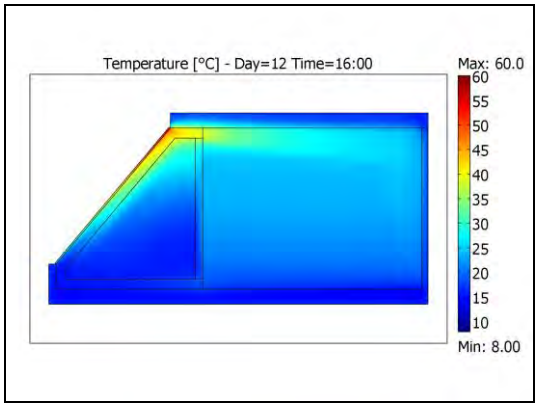

Figure 12. Thermal map (day 12 – time 16:00).

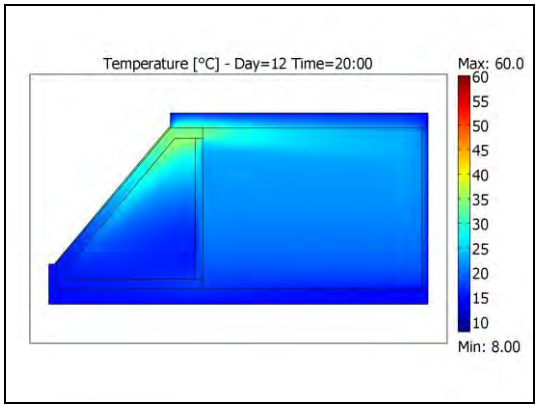

Figure 13. Thermal map (day 12 – time 20:00).

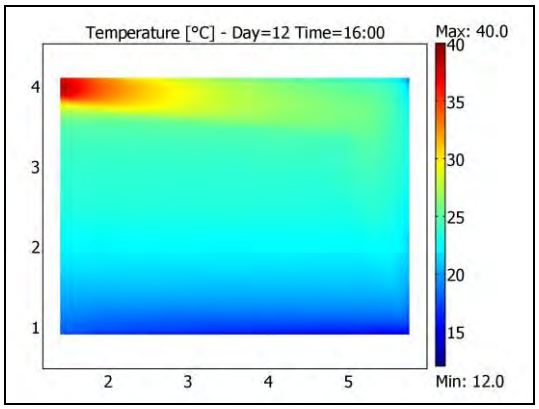

Figure 14. Thermal map of indoor air (day 12 – time 16:00).

Globally, the maximum temperature gradient of indoor air temperature amounts to 18 °C. However, referring to the acceptable conditions for thermal comfort, measurements of thermal gradient have to be computed in the portion of the room occupied by people. Figure 15 reports, for several horizontal positions, the temperature value as a function of the height. It can be observed as, for height between 0.5 m and 2.5 m from the floor, thermal gradient in vertical direction is almost constant and its value is 2°C/m about. Even if thermal gradient in the portion of the room occupied by people results smaller than the global value referred to all the indoor air, it is higher than the standard value advised for thermal comfort (0.5 °C/m).

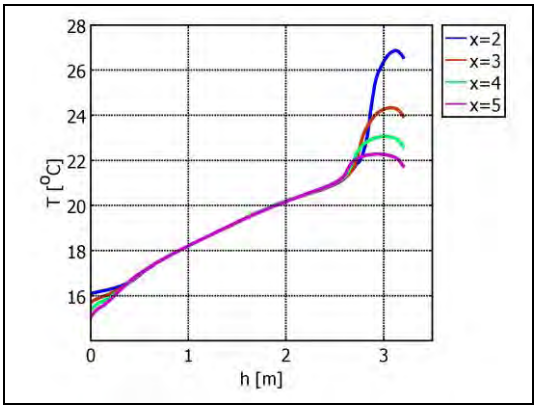

Figure 15. Thermal map of indoor air (day 12 – time 16:00).

The last aspect we examined concern the effectiveness of the thermal mass storage. In Table 2 the relative percentage in volume of concrete and air where temperature is higher than 20 °C is reported for several hours.

Percentage of volume where T > 20°C (day 12)

Time	Concrete	Air
00:00	34%	40%
04:00	33%	20%
08:00	**32%**	**18%**
12:00	35%	64%
16:00	37%	**83%**
20:00	**37%**	73%

Table 1: Percentage of concrete an air volume where T is higher than 20 °C.

From reported data two considerations can be done. Firstly, during time the thermal inertia of concrete is appreciable: in spite of great variation of temperature detected in air, the concrete volume appears almost isothermal. Secondly, it appears that just a portion of the thermal volume (the upper portion, see pictures reported in Figures 10-13) reaches "high" thermal level.

4. Conclusions

This study concerns a numerical investigation on fluid-dynamical and thermal behavior of a passive solar system for indoor heating, whose the functional principle is based on the thermo-syphon circulation. The distributed numerical approach has allowed to detect strong and weak points for this kind of system. The first one can be resumed in the free thermal gain obtained in the heated volume, that is combined with a favorable time displacement of indoor temperature variation with respect to the external thermal load. On the other hand, a high temperature stratification has been detected that could induce discomfort conditions for occupants. The effectiveness of thermal storage mass has been investigated also, showing that just a portion of the storage mass results really contributive. It appears that further analyses on this topic are needed in order to optimize the studied system.

5. References

1. J. Onishi, H. Soeda, M. Mizuno, Numerical study on a low energy architecture based upon distributed heat storage system, *Renewable Energy*, vol. 22, pp. 61-66, 2001.

2. V. Hernandez, D. Morillon, R. Best, J. Fernandez, R. Almanza, N. Chargoy, Experimental and numerical model of wall like solar heat discharge passive system, *Appl. Thermal Engineering*, vol. 26, pp. 2464-2469, 2006.

3. J. Shen, S. Lassue, L. Zalewski, D. Huang, Numerical study on thermal behavior of classical or composite Trombe solar walls, *Energy and Buildings*, vol. 39, pp. 962-974, 2007.

4. L. Zalewski, M. Chantant, S. Lassue, B. Duthoit, Experimental thermal study of a solar wall of composite type, *Energy and Buildings*, vol. 25, pp. 7-18, 1997.

5. A. Chel, J.K. Nayak, G. Kaushik, Energy conservation in honey storage building using Trombe wall, *Energy and Buildings*, vol. 40, pp. 1643-1650, 2008.

6. B. Zamora and A.S. Kaiser, Thermal and dynamic optimization of the convective flow in Trombe Wall shaped channels by numerical investigation, *Heat Mass Transfer*, vol. 45, pp. 1393-1407, 2009.